Stability and Modification of Polyglutamate Langmuir–Blodgett Bilayer Films

Vladimir V. Tsukruk,*,† Mark D. Foster,† Darrell H. Reneker,† Albert Schmidt,‡ Hong Wu,† and Wolfgang Knoll‡

The Institute of Polymer Science, The University of Akron, Akron, Ohio 44325-3909, and the Max-Planck-Institut für Polymerforschung, Postfach 3148, D-6500 Mainz, Germany

Received August 9, 1993; Revised Manuscript Received November 8, 1993®

ABSTRACT: Langmuir–Blodgett bilayers of a polyglutamate (PG) statistical copolymer have been investigated using atomic force microscopy (AFM) and X-ray reflectivity. PG ordered bilayer films on silicon surfaces possess an "expanded" thickness of 4.12 ± 0.05 nm and an average roughness of 0.7 ± 0.2 nm. Possibilities for surface modification by the AFM tip were explored. Formation of an "abrasion" surface morphology was related to a stick-slip mode of the AFM tip movement. Using the AFM tip, several surface modifications were investigated: fabrication of large (several hundreds of nanometers) and small (several nanometers) holes; "writing" of grooves of predictable geometry; fabrication of holes of single layer and bilayer depth; cleaning of the surface and fabrication of holes inside this new area. The anisotropic mechanical properties of the PG bilayer were probed and attributed to orientation of the PG backbones along the dipping direction. The dynamic behavior of the surface changes were observed as well.

Introduction

Polyglutamates (PG) of the "hairy-rod" type having rigid rod-like backbones and flexible aliphatic side chains possess a unique set of physical properties and can form ordered molecular films with high optical anisotropy, suitable for optical waveguide applications.[1-3] In "as-deposited" multilayered Langmuir–Blodgett (LB) films the molecules form bilayers lying parallel to the substrate surface.[3,4] Strong preferential orientation of the PG backbones along the dipping direction is induced by the vertical transfer technique.[5-7] This causes anisotropy of the birefringence in the plane of prepared LB films. The formation of a "bundle" morphology oriented along the dipping direction in LB films of octadecyl-substituted PG and modification of their surfaces were recently observed by atomic force microscopy (AFM).[8-14]

AFM provides the possibility not only for direct observation of surface morphology with nanometer resolution at ambient conditions but also for active modification of the surface by mechanical interaction with the AFM tip.[15,16] The durability of soft polymeric surfaces during interaction with the AFM tip is a crucial question in the reproducibility and interpretation of STM and AFM images. Many examples of artifacts observed on polymer surfaces have been recently recognized.[15] The local, managed modification of the surfaces by controlled scanning with high forces has been demonstrated recently for a few polymeric materials and LB films from organic compounds.[8,15,16] Surface modification and observation of local mechanical properties are reported here for soft LB bilayer films based on PG.

An asymmetric model proposed for intralayer structure in multilayered films[1,3,7] considers the bilayers to have the PG backbones forming a dense central core and the alkyl side chains located in the outer layers. In this model the core has ca. 1-nm thickness and the surface of the bilayer is composed of alkyl chains with liquid-like ordering.[7] Driving forces for formation of this molecular packing are the hydrophobic–hydrophilic interactions of both the side chains and the PG backbones with the air–water interface during formation of the monolayers. The internal structure of a single bilayer deposited on a silicon surface could differ dramatically from the structure of the same bilayer in multilayered films. Nevertheless, the lack of quantitative structural data for PG LB films makes it impossible to verify the correct model for molecular packing in the PG bilayers. This point will be addressed here using the combined power of X-ray reflectivity and AFM experimental techniques.

Chart 1

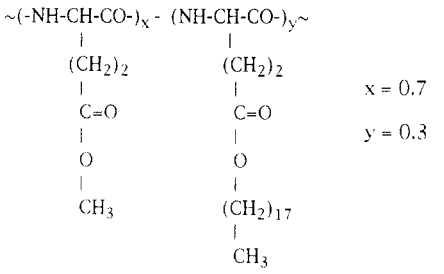

Experimental Section

The present study is of an octadecyl-substituted PG (poly(γ-methyl L-glutamate-*co*-γ-octadecyl L-glutamate)) with a degree of substitution of ca. 30%, which is noncrystalline at room temperature. The chemical structure of these molecules is shown in Chart 1. The synthesis of PG has been described elsewhere.[5,17] PG bilayers (see Chart 2) were deposited on hydrophobized polished substrates cut from silicon wafers according to a procedure described earlier.[9] Images of the surfaces at ambient temperature were obtained with an atomic force microscope, the Nanoscope II (Digital Instruments, Inc.), using a pyramidal Si_3N_4 tip. Scanners D and A were used for scanning on scales from 15 μm to 10 nm with applied forces in the range 20–60 nN except for special experiments with higher forces. Data about the average thickness and macroscopic roughness of PG bilayers were obtained independently from X-ray reflectivity measurements (for details, see ref 18). The reflectometer used vertical slit collimation with a pyrolytic graphite primary monochromator ($\Delta\lambda/\lambda$ = 0.015 for the *Cu* Kα radiation used) and a scintillation detector. The nominal resolution (fwhm) at an incident angle

* To whom correspondence should be sent. Present address: Department of Engineering Technology, College of Engineering and Applied Sciences, Western Michigan University, Kalamazoo, MI 49008.

† The Institute of Polymer Science, The University of Akron, Akron, OH 44325-3909.

‡ Max-Planck-Institut für Polymerforschung, Postfach 3148, D-6500 Mainz, Germany.

® Abstract published in *Advance ACS Abstracts*, January 15, 1994.

0024-9297/94/2227-1274$04.50/0

Chart 2

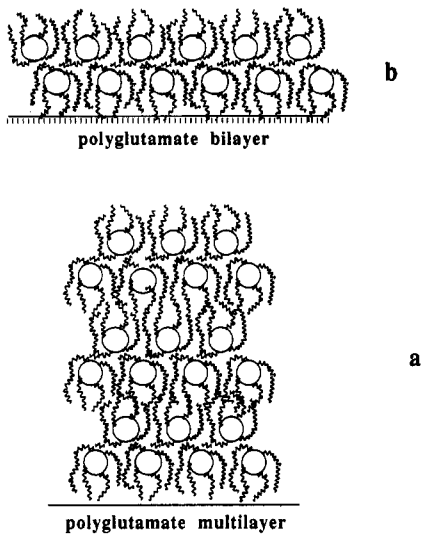

of 1° was $\Delta q = 0.02\ \text{nm}^{-1}$ ($q = 4\pi \sin\theta/\lambda$, where 2θ is the scattering angle and λ is the wavelength).

Results and Discussion

X-ray reflectivity measurements were performed for three different samples of LB films obtained at similar conditions. The obtained experimental data for all films are self-consistent. Numerical data discussed below were obtained by averaging of parameters obtained for all three samples. X-ray reflectivity data and best fit for a PG bilayer on silicon are presented in Figure 1. The data display two very broad interference maxima superposed on the rapidly decreasing Fresnel curve for the silicon surface. Constrained nonlinear regression of the data for the three samples using a simple model of a single homogeneous film yields a bilayer thickness of 4.12 ± 0.05 nm, which is much higher than the average thickness of a PG bilayer in multilayered LB films or in composite LB films (3.45 ± 0.05 nm).[18] Regression of the data using a more complex model distinguishing between regions rich in both backbones and side chains yields comparable values for overall thickness and interface roughness. However, the spatial resolution of the data presented here, which is limited by the scattering intensity at higher angles, is insufficient to unambiguously argue for the more complex model of internal structure. The surface roughness, averaged over ca. 1 cm^2 of surface area and over three samples, is 0.7 ± 0.2 nm. This agrees with values obtained recently for multilayer PG LB films.[18]

The greater thickness of the PG bilayer studied here may be rationalized by noting the very different environments seen by this bilayer on the silicon surface and in multilayer films. In the multilayer film each interior bilayer interacts with two neighboring layers of the same type (Chart 2). A model suggested for the as-deposited multilayer structure[7] (see Chart 2a) has two important features. First, the PG backbones and side chains are located preferentially in the center of the bilayer, and the alkyl chains form soft regions adjoining the boundaries of the bilayer. A second key feature of this structure is the extensive interdigitation of the side chains from adjacent bilayers.[18] This interdigitation results in a substantial reduction of the average periodicity in electron density normal to the surface as compared to a model without any interdigitation. When a bilayer stands alone on a substrate, as sketched in Chart 2b, the opportunity for interdigitation is lost. The bilayer then adopts a thickness between that characteristic of the strongly interdigitated multilayer structure and that of a bilayer containing closely packed backbones and fully extended alkyl side chains (ca. 5.2 nm as estimated from molecular modeling). To elaborate this model, additional X-ray reflectivity experiments with a higher spatial resolution are needed.

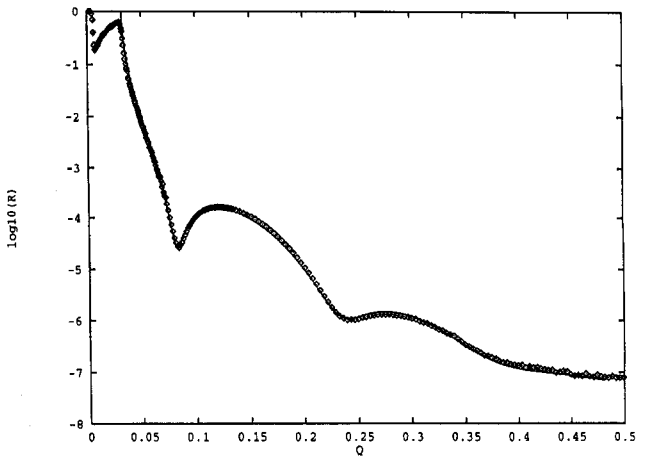

Figure 1. X-ray reflectivity, R, for a bilayer of PG on silicon as a function of q_z ($=4\pi \sin\theta/\lambda$), the component of the scattering vector perpendicular to the sample surface. Broad interference maxima observed are characteristic of a rather thin film. Shown also is the simulated reflectivity expected from a layer of thickness 4.12 ± 0.05 nm, air–layer roughness of 0.7 ± 0.2 nm rms, and layer–substrate roughness of 0.36 ± 0.04 nm rms.

Detailed descriptions of a variety of surface morphologies for various PG bilayers and corresponding composite LB films have been presented elsewhere.[9] A typical first-scan AFM image for such a film with selected naturally occurring defects, e.g., an irregular hole of 1.6-nm depth corresponding to a missing piece of a single PG layer, is presented in Figure 2a. The local PG surface roughness averaged over 1 μm × 1 μm squares is 0.3 ± 0.1 nm, which is comparable to that of the supporting silicon surface. Increasing the scale over which roughness is calculated to 4 μm × 4 μm includes some macroscopic defects and gives a roughness value of 0.9 ± 0.2 nm, which corresponds well with average rms roughnesses derived from X-ray data for macroscopic area.

Interaction of the PG bilayer with the AFM tip leads to minor damage of the surfaces even for the first scan as indicated by shallow grooves in the image (Figure 2a). Preferential orientation of macroscopic features along the dipping direction (vertical in Figure 2a) is observed. More dramatic changes in surface morphology are observed for PG bilayers on silicon after succeeding scans when the scanning direction is perpendicular to the dipping direction (Figure 2b–d). Very gentle scanning with minimum force (~20 nN) leads to visible changes of the surface morphology from scan to scan. The development of heterogeneous surface morphology is observed as an increase in height of the ridges, leading to an increase in microroughness to 0.8 ± 0.1 nm for the second scan and 1.1 ± 0.1 nm for the third scan. The stability of these morphological features is demonstrated in Figure 2b, where the scanning direction has been rotated by 45°. Prolonged scanning leads to a very rough surface with a local roughness of 3 ± 0.8 nm and ridge heights of 8–15 nm (Figure 2c,d). Apparently, this corresponds to complete destruction of the initial bilayer surface and formation of a heterogeneous surface with the pieces of bulk material concentrated in high ridges aligned along the dipping direction. This oriented morphology is known as an "abrasion pattern" and was recently observed by AFM for PG films and amorphous polystyrene films.[8,9,19]

Gradual development of the surface heterogeneity is visible in Figure 2d, where the number of scans increases gradually from one (roughness is 0.4 nm) for the upper

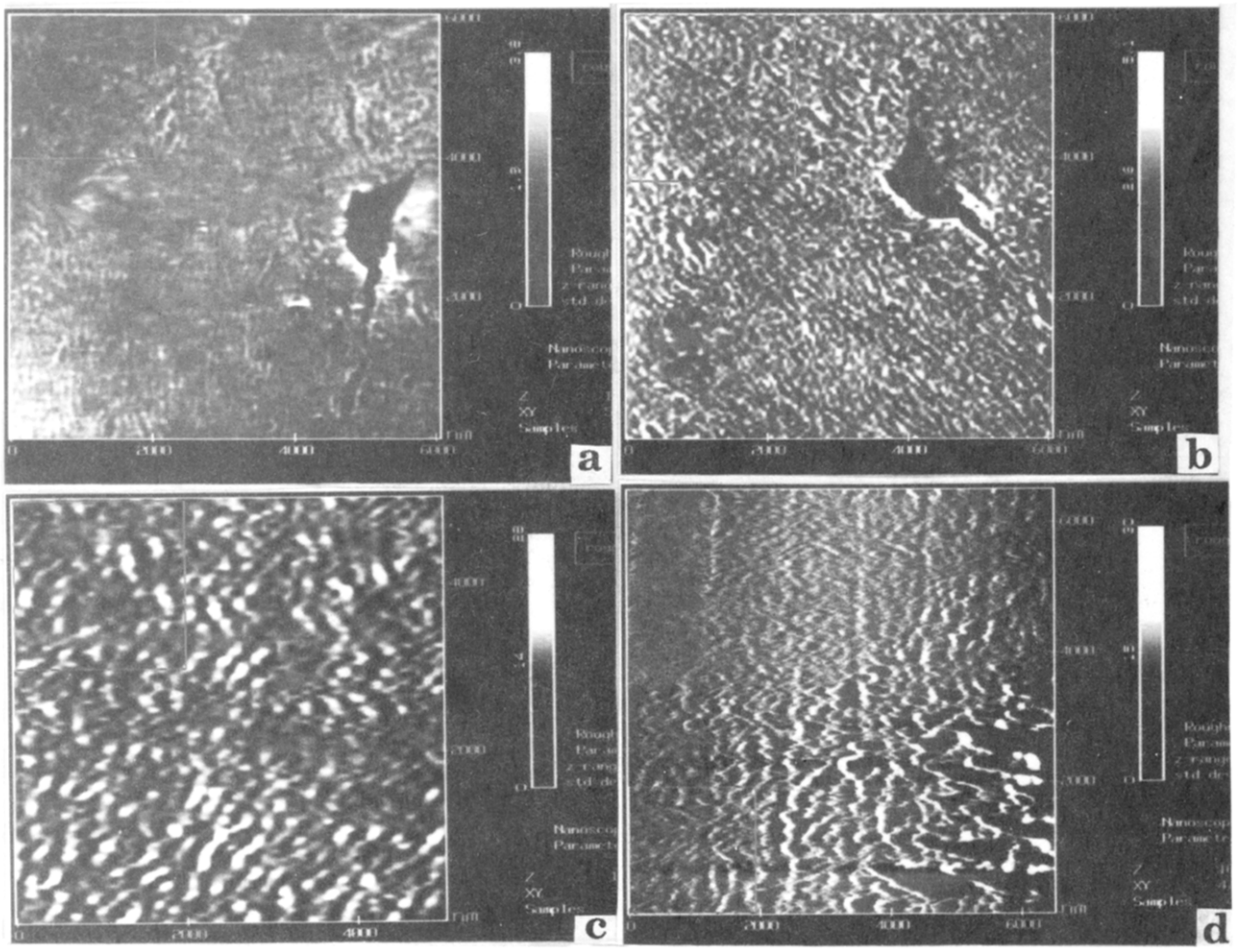

Figure 2. Development of surface morphology with repeated scanning for a PG bilayer deposited directly on silicon: (a) First scan of the area on a large scale (6 μm × 6 μm). The rms roughness on the 1-μm square is 0.3 nm. The vertical direction corresponds to the dipping direction and the scanning direction is transverse to the dipping direction. (b) Second scan of the same area (6 μm × 6 μm), rotated by 45°. The development of the ridges aligned along the dipping direction is visible. The rms is 0.5 nm. (c) PG bilayer film after four scans (6 μm × 6 μm). The rms roughness is 1.5 nm. (d) Image (6.5 μm × 6.5 μm) of scans shifted step-by-step along the x- and y-axes by 1.2 μm. The scans are divided by visible vertical borders. The left upper corner represents the surface after one scan and the right bottom corner represents an image of the film after twelve scans.

left corner to twelve (roughness is 3 nm) for the lower right corner. Borders between succeeding scans, shifted in the horizontal direction by 1.2 μm per scan, are also observed. Development of the heterogeneous surface depends very strongly upon the scanning parameters used: force applied, number of scans, and the tip velocity. The roughness of the PG film increases sharply with increasing tip velocity (or regime of scanning when image size increases while retaining the tip velocity) (Figure 3). The roughness increases steadily and almost linearly for number of scans from 2 to 8 if the tip velocity is kept very low (less than 0.8 μm/s) and unchanged. This is similar to the dependences observed before for polystyrene films.[19] Under these conditions, the PG films are distorted after 10 scans when roughness exceeds the thickness of a monolayer (Figure 3a). The distance between the ripples formed depends also upon tip velocity with a tendency to increase at higher velocities.

The observed roughness averaged over 1-μm size area depends strongly upon the tip velocity (Figure 3b). The rms decreases sharply with a decrease in scanning rate from 2 to 0.3 μm/s. On the other hand, increasing the scanning rate to more than 10 μm/s also leads to a significant decrease of "roughness" (Figure 3b). This behavior is more pronounced for the third scan. For velocities in the 2–10 μm/s range, the roughness is almost constant for the first scan. The measured variations in rms reflect the features of the tip–bilayer mechanical interactions. Instabilities of the tip movement cause increasing roughness of the films while stable sliding of the tip preserves initial surface smoothness. Periodic heterogeneities on the surface could be formed by friction instabilities of the sliding surfaces of the so-called stick-slip type.[20–23] In this type of movement changes in the surface sliding are connected with periodic transitions between "static" (solid-like) and "kinetic" (fluid-like) states, which are analogous to freezing–melting transitions.[20] Minor variation of shearing force is needed to produce expected jumps from one state to another. The observed dynamical behavior for PG bilayers is consistent with general relationships expected for stick-slip friction phenomena. The existence of such a mechanism in our system may be related to the occurrence of a solid–liquid transition in bulk PG for the side alkyl chains at ≈290 K,[22] which is very close to ambient temperature. We could speculate that this phase transformation occurs in PG bilayers in this range of temperatures as well, although we have no independent experimental evidence of this.

One feature of the stick-slip mode is its disappearance at velocities above a critical velocity of shearing v_c. For a crude estimation of the critical velocity, a simple relation can be used:[20,21] $v_c \sim 0.05(rF/F_t)^{1/2}$, where r is a characteristic lattice dimension, F is the static friction force, and F_t is the force load to the AFM tip. If the same dependence between load and friction forces is assumed for PG bilayers with alkyl chains located at the surface (Chart 2) as has been for the hexadecane films studied in ref 20, then for our experimental conditions we get $v_c \sim 10$–15 μm/s. This

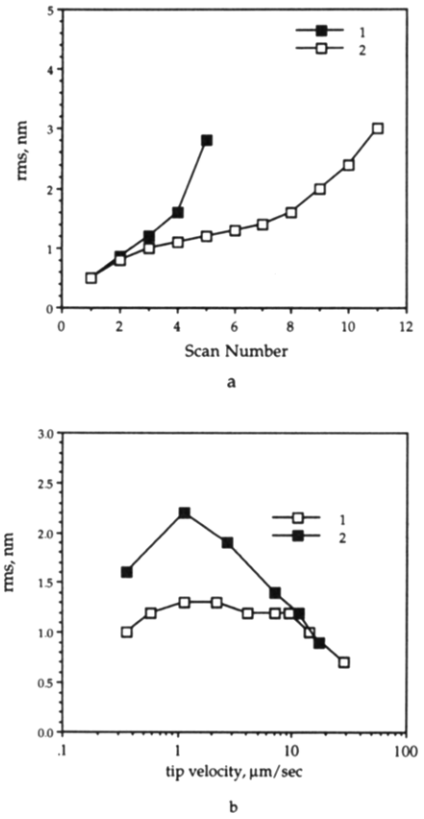

Figure 3. Development of the PG bilayer surface roughness as a function of various scanning parameters: (a) rms roughness versus number of scans for (1) increasing tip velocity from 1 to 5 μm/s and (2) constant scanning rate of 0.8 μm/s; (b) dependence of the roughness in the 1 μm × 1 μm area on tip velocity (1) first scan; (2) third scan).

estimation fits quite well with the observed decrease of rms surface roughness for tip velocities higher than 10 μm/s (Figure 3b). The nonmonotonic dependence of rms roughness upon sliding velocity in the interval from 0.2 to 50 μ/ms is very similar to the behavior of the sliding surfaces described in ref 20. Finally, smearing of surface features at higher tip velocities can be partially due to electronic feedback delay. The integral gain was kept in the 0.2–0.5 range, and the proportional gain was not more than 0.5.

When scanning in the direction parallel to the dipping direction, an abrasion pattern is not formed. The first scan leads to a random surface roughness (Figure 4a). This reflects the anisotropic frictional properties of PG films due to parallel orientation of the backbones in one direction. In Figure 4a, the central square region, which has been scanned in the parallel direction, may be compared with areas that have been scanned transverse to the dipping direction. Instead of a highly oriented abrasion morphology, random height deviations in the 0.4–0.6-nm range are observed in the central region. The local microroughness in this area increases almost steadily for the first three scans from 0.4 to 0.9 nm in a manner similar to that discussed above. Succeeding scans with increasing sizes can produce square patterns at the PG bilayer surface (Figure 4b).

Application of higher forces during scanning in selected regions of soft organic film leads to local scraping of the sample.[8,9,15,16] These modifications on a molecular scale have been done only for organic molecular films with isotropic in-plane organization of small molecules. Several possible modes of nanomachining of such highly anisotropic material such as PG bilayers by the AFM tip were investigated: cleaning of the surface and fabrication of holes inside a hole; fabrication of large (several hundreds of nanometers) and small (several nanometers) holes; "writing" of grooves of desirable geometry; fabrication of holes of single layer and bilayer depth; and fabrication of anisotropic holes by scanning along and transverse to the PG backbone alignment. The surface modifications can be observed by a subsequent scan over a larger area using a low force.

Very smooth areas of PG bilayers free from high ridges can be produced by scanning with modest (60–100-nN range) forces (see these areas of different sizes in Figure 5a). High ridges at the edges of the areas are caused by the accumulation of scraped material. Small holes up to 10-nm size were produced inside this area at selected locations on the bilayer film (Figure 5b). The depth of these square holes is 2.0 ± 0.3 nm, which is close to the PG single-layer thickness, known from X-ray data (2.1 nm; see above). Thus, during cleaning of the PG bilayer surface, only the single upper layer of PG is scraped, while the second, bottom layer is still preserved.

Use of higher force during scanning of a virgin bilayer film leads to the tip piercing through only the upper PG layer of the entire bilayer, depending upon the force applied. This causes formation of holes of different depths (Figure 5c). The average depth of holes penetrating through the upper layer only is 2.1 ± 0.2 nm and the depth of holes extending through the whole bilayer is 4.0 ± 0.3 nm, as can be seen from the cross-section in Figure 5d. These values coincide very well with the average thickness of the PG bilayer film determined from X-ray data and

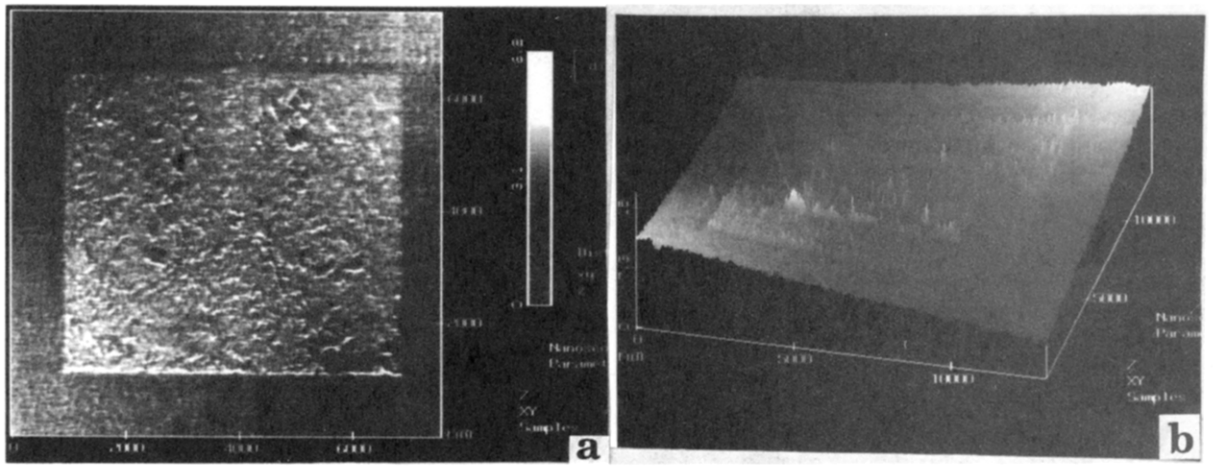

Figure 4. (a) AFM image (8 μm × 8 μm) of a square region with random rugosity produced on the bilayer surface during the previous scan with scanning parallel to the dipping direction (in the central 6 μm × 6 μm region); (b) the same area as in (a), imaged by a third scan on the 13 μm × 13 μm scale.

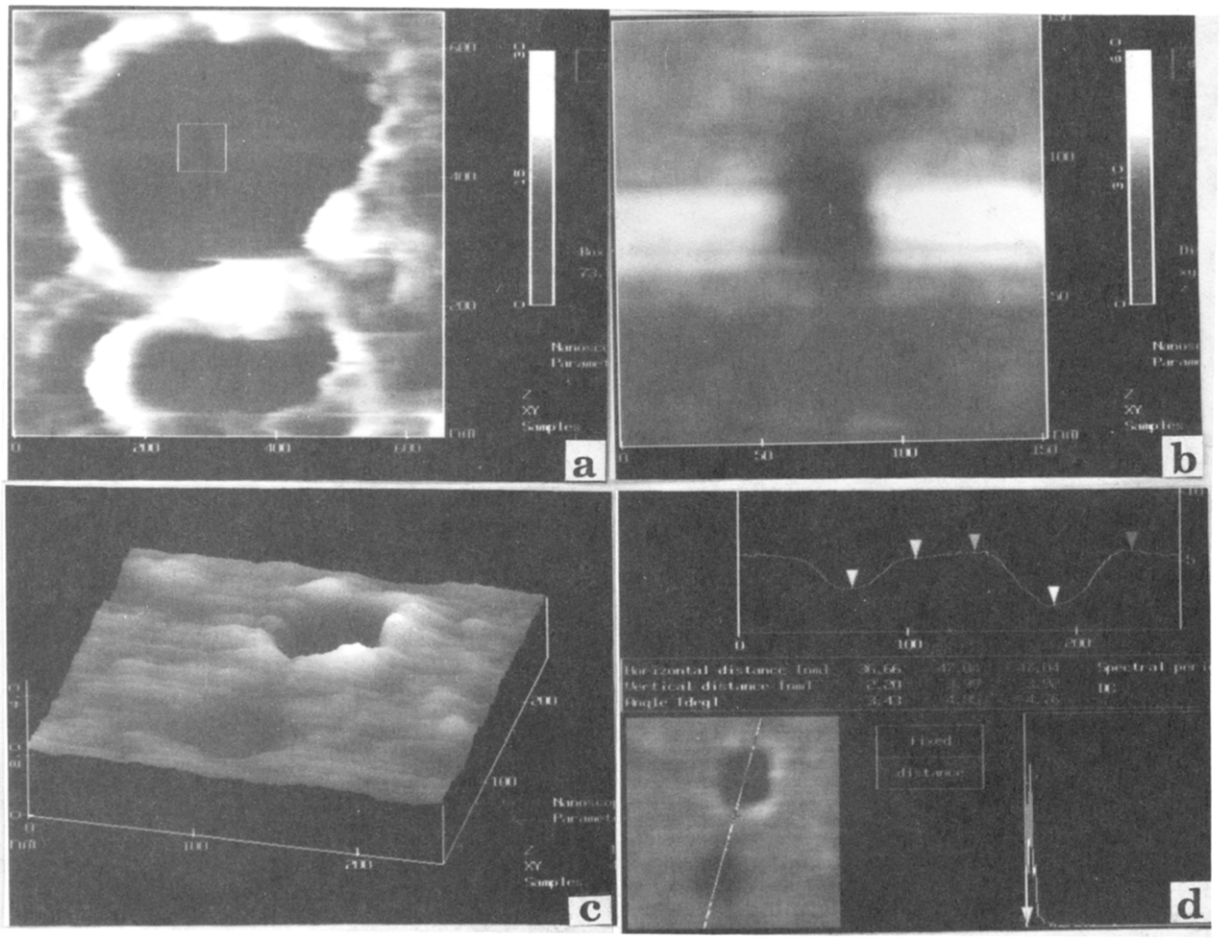

Figure 5. Various modifications of the PG bilayer surface: (a) 650 nm × 650 nm image of two neighboring smooth areas produced in a PG film by scanning with modest forces. Inside the larger area, near the center (marked by light square), a second hole 30 nm × 30 nm across and 2 nm deep was produced. This hole is enlarged in (b), 150 nm × 150 nm scan size. (c) Two different holes produced in a PG film using different forces, 250 nm × 250 nm scan size: a hole only in the upper PG layer with 30 nm × 30 nm lateral size and 2-nm depth and a hole through the whole bilayer with 50 nm × 50 nm lateral size and 4-nm depth, produced by higher forces. (d) Cross-section of these holes of different depths.

confirm the models of "expanded" molecular packing described above (Chart 2). The cross-section profiles of the small holes are not truly rectangular as can be expected for an ideal needle tip but are of a smooth, parabolic-like shape (Figure 5d). Evidently, this reflects the real shape of the AFM tip with an end which is not atomically sharp as has been discussed elsewhere.[9,14,15] If we consider the profiles to be additive functions of the tip end shape and scan size, the radius of curvature for the pyramidal tip used can be estimated as 30 nm.

By increasing the scanning area, larger holes can also be made (see the example of a 400 nm × 400 nm hole in Figure 6a). The main difference between the shape of the large and small (<50 nm) holes is the presence of high ridges of scraped material at the edges for all large holes produced (see Figure 6a, for example). In contrast, small rectangular holes have very smooth edges (Figure 5c). This probably reflects different mechanisms of hole formation for different spatial scales. Scanning over large areas with relatively high tip velocity digs out soft material. In contrast, applying high forces over a small scanning area covering only 3–4 macromolecular backbones pushes aside the macromolecules, penetrating through the soft layers and forming a smooth shallow hole by a local structural rearrangement of the backbones.

Several attempts were made at "writing" on the PG bilayer surface in a manner similar to that demonstrated recently for LB films from low molecular mass organic compounds.[8,15,16] In Figure 5b the trace of the letter "U" produced by scanning with higher forces is shown. The rodlike backbones are aligned in the vertical direction and the AFM tip moves parallel to this direction. While vertical grooves of 20-nm width (produced by controlled displacements of the scanning area) are quite straight, any attempts to change the direction of the grooves by shifting the image center along the x-direction failed (Figure 6b). This can be connected with the high anisotropy of mechanical properties of bilayer PG films due to their internal molecular nematic-like ordering. In the nematic phases composed of PG macromolecules, the rodlike backbones possess a long-range orientational ordering and short-range positional ordering in the lateral packing of the backbones.[24] Transverse displacements of the PG backbones, caused by mechanical interactions with the AFM tip, can be accomplished by local rotation, bending, and diffusion of the macromolecular segments. Such local molecular motion in the direction parallel to the backbones is much more difficult. In this case backbone motions cost more energy than local segmental displacement.

Additional evidence for anisotropic mechanical properties of PG bilayer films with much higher stability for probing along the dipping (molecular) direction comes from a scraping test, which causes formation of locally anisotropic holes (Figure 6c,d). If the tip is moving transverse to the PG backbones, square holes of various sizes can be produced easily (Figure 6c). When the tip is moving parallel to the PG backbone alignment, a highly anisotropic hole shape results (Figure 6d). In this case the hole size in the y-direction (transverse to the PG backbone orien-

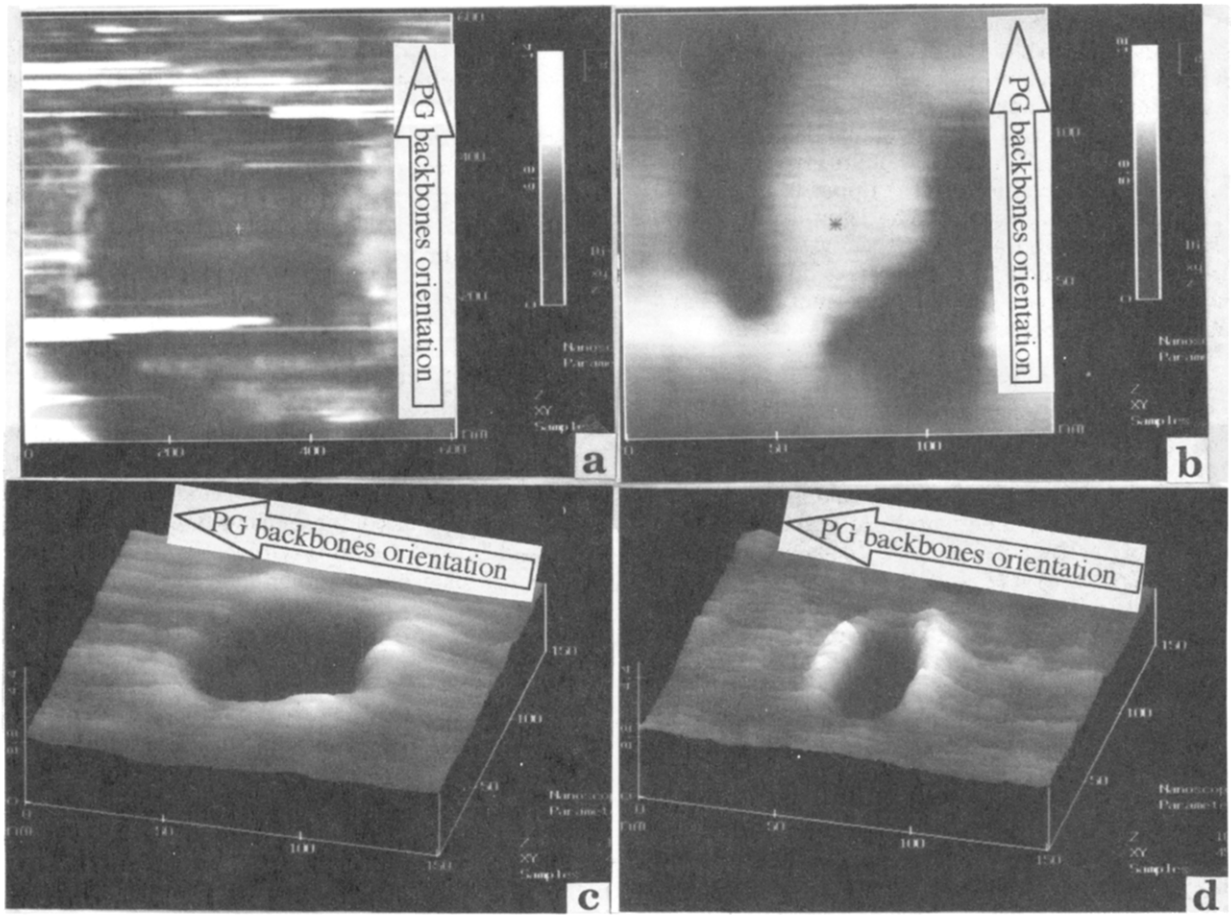

Figure 6. Various modifications of PG bilayer surfaces: (a) square hole of 400 nm × 400 nm size and one layer depth, 600 nm × 600 nm scan size. (b) Grooves produced by a controlled shift of the scanning area (20 nm × 20 nm) to create the letter "U", 150 nm × 150 nm scan size. (c) Square hole in a PG bilayer of 4.0 ± 0.3 nm depth and 50 nm × 50 nm lateral size produced with the scanning direction perpendicular to the aligned PG backbones (horizontal on the image), 150 nm × 150 nm scan size. (d) Anisotropic hole in a PG bilayer of 4.0 ± 0.3 nm depth and 50 nm × 20 nm lateral size produced by scanning (in an area of 50 nm × 50 nm) parallel to the PG backbones (horizontal on the image), 150 nm × 150 nm scan size. The hole size along the backbone direction is smaller by a factor of 2.5.

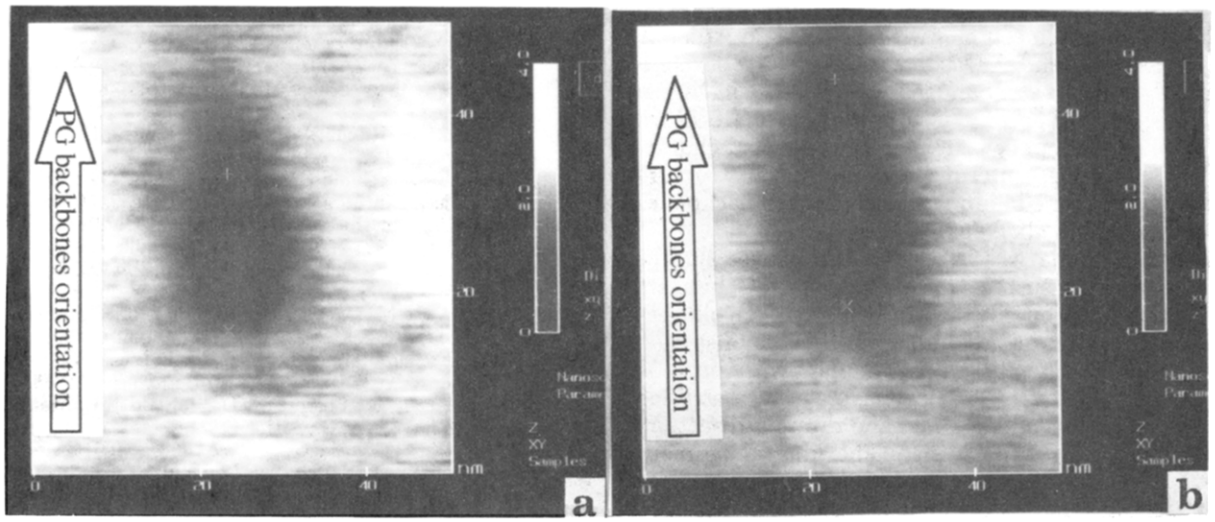

Figure 7. Top view of a hole (scan in 20 nm × 20 nm area) in the PG bilayer film right after manufacture (a) and 1 h later (b).

tation) corresponds to the scan size (50 nm in Figure 6d), but the hole size along the backbone direction is much smaller (only 20 nm). Thus, the same level of applied forces to a tip along the PG backbones leads to much less surface distortion, and in-plane mechanical anisotropy of the layers affects the shape of the holes that are produced. Thus, the mechanical tests made including the variation of roughness, the "writing" test, and the fabrication of holes give evidence of anisotropic mechanical properties of PG films. This high anisotropy, with higher resistance to local mechanical distortion in the direction parallel to the direction of the PG backbones, is a consequence of the high orientational order of PG backbones in LB bilayers.

As mentioned before, the PG is a very soft material at room temperature with nematic-like ordering.[1,2] The PG center-of-mass translational diffusion coefficient in the direction perpendicular to the layer plane in an LB film has been estimated from a neutron reflectivity study[18,22,25] to be less than 10^{-18} cm^2/s. For such soft, mesomorphic materials one can expect that the dynamical behavior of

surface features can be observed because nanometer-scale diffusion can occur in time intervals of a few hours. By comparison, fast diffusion on metal surfaces allows surface reconstructions in time intervals of a few seconds.[14] Preliminary observations of the dynamic behavior of PG films during time intervals of a few hours give ambiguous results. For a hole produced in the upper layer of a PG film (Figure 7, 2.0-nm depth), the horizontal and vertical dimensions increase 30–40% for the first 20 min and remain virtually unchanged for the next hour. Further observations were accompanied by systematic shifts and thermal drift of the images and interactions with the AFM tip.

It seems that the initial increase of hole size is promoted by mechanical interactions with the AFM tip. The absence of a visible decrease in hole size for the next hours can be attributed to very restricted diffusion of the macromolecules in the plane of the bilayer films. Taking into account the accuracy in measurements of the lateral sizes, we can estimate the upper limit of detectable diffusion coefficient in the plane of the bilayer D. As known, a crude estimation of D can be done if one is able to measure displacement of molecular features δ over a period of time τ.[26] The random walk approximation gives an equation for $D \sim \delta^2/\tau$.[26] Taking into account the accuracy of the measurements of the size dimensions in our particular case (ca. ±2 nm), from this relationship we can estimate that any changes of the hole sizes associated with lateral diffusion for the period of observation ($\tau \sim 10^4$ s) and diffusion coefficient more than 10^{-18} cm^2/s should be easily detected with our technique. Our results, namely, the absence of a visible variation in hole size, therefore suggest that either the real diffusion coefficient D for PG bilayers is much smaller than this limit ($\ll 10^{-18}$ cm^2/s) or free diffusion of maromolecular fragments is disturbed by strong interaction with the AFM tip.

Conclusions

The surface properties of PG bilayers deposited on silicon substrates have been investigated and several possibilities for nanomachining with the AFM tip explored. X-ray reflectivity and AFM observations corroborate a picture of a single "expanded" PG bilayer having a thickness greater than that seen in multilayer LB films. The PG bilayer adopts a thickness between that characteristic of the strongly interdigitated multilayer structure and that of a bilayer containing closely packed backbones and fully extended alkyl side chains.

Interaction of the AFM tip with the bilayer surface generally leads to surface roughening for PG bilayers deposited directly on silicon. In contrast, PG bilayers deposited on cadmium arachidate multilayers display a greater mechanical stability during scanning with the AFM tip.[9] This roughening of the PG bilayers is more striking when scanning perpendicular to the dipping direction, which is also the direction of the PG backbone alignment along the dipping direction. The observed roughness varies with the scan rate. The initial roughness increases somewhat with the scan rate for tip velocities of 0.2–8 μm/s and then drops sharply, suggesting the existence of a critical scan velocity below which a stick-slip mechanism is active.

Several features of nanometer sizes down to 10 nm across can be produced in the bilayers using the AFM tip, each feature being sensitive to the anisotropic nature of the layers. A crude estimation for the upper limit of diffusion coefficient for PG movement in the layer plane ($<10^{-18}$ cm^2/s) was obtained by analysis of machined hole time evolution. This small value is consistent with very low estimates of the diffusion coefficient perpendicular to the layer plane obtained from neutron reflectivity measurements.[22] Obviously, that future study of anisotropic mechanical properties of PG bilayers should include lateral force microscopy and surface force measurement techniques as the most appropriate tools for probing of macroscopic and microscopic mechanical properties of molecular films.

Acknowledgment. Funding for this research through the National Science Foundation (Grant CTS-9110110) and BMTF is gratefully acknowledged. The authors are very grateful to Prof. G. Wegner and Dr. K. Mathauer (MPI, Mainz) for supplying the polyglutamate and helpful discussions, Prof. J. Israelachvili (University of California, Santa Barbara) for discussion of the stick-slip sliding mode and supplying his comprehensive papers on this topic (ref 20), and Dr. F.-J. Schmitt (University of California, Santa Barbara) for useful comments on our manuscript.

References and Notes

(1) Duda, G.; Wegner, G. *Makromol. Chem., Rapid Commun.* **1988**, *9*, 495.
(2) Mathauer, K.; Mathy, A.; Bubeck, C.; Wegner, G.; Hickel, W.; Scheunemann, U. *Thin Solid Films* **1992**, *210/211*, 449.
(3) Menzel, H.; Weichart, B.; Hallensleben, M. L. *Thin Solid Films* **1993**, *223*, 181.
(4) Hickel, W.; Duda, G.; Jurich, M.; Krohl, T.; Rochford, K.; Stegeman, G. I.; Swalen, J. D.; Wegner, G.; Knoll, W. *Langmuir* **1990**, *6*, 1403.
(5) Mathy, A.; Mathauer, K.; Wegner, G.; Bubeck, C. *Thin Solid Films* **1992**, *215*, 102.
(6) Schwiegk, S.; Vahlenkamp, T.; Xu, Y.; Wegner, G. *Macromolecules* **1992**, *25*, 2513.
(7) Lee, S.; Dutcher, J. R.; Stegeman, G. I.; Duda, G.; Wegner, G.; Knoll, W. *Phys. Rev. Lett.* **1993**, *70*, 2427. Menzel, H.; Hallensleben, M. L.; Schmidt, A.; Knoll, W.; Fisher, T.; Stumpe, J. *Macromolecules* **1993**, *26*, 3644.
(8) Chi, L. F.; Eng, L. M.; Graf, K.; Fuchs, H. *Langmuir* **1992**, *8*, 2255.
(9) Tsukruk, V. V.; Foster, M. D.; Reneker, D. H.; Schmidt, A.; Knoll, W. *Langmuir* **1993**, *9*, 3538.
(10) Sarid, D. *Scanning Force Microscopy*; Oxford University Press: New York, 1991.
(11) Schwarz, D. K.; Garnaes, J.; Viswanathan, R.; Zasadzinski, J. A. *Science* **1992**, *257*, 508.
(12) Viswanathan, R.; Schwartz, D. K.; Garnaes, J.; Zasadzinski, J. A. *Langmuir* **1992**, *8*, 1603.
(13) Hansma, H. G.; Could, S. A.; Hansma, P. K.; Gaub, H. E.; Longo, M. L.; Zasadzinski, J. A. *Langmuir* **1991**, *7*, 1051.
(14) Proceedings of the VIth International Conference on STM, Switzerland, 1991 (*Ultramicroscopy* **1992**, *42–44*).
(15) Frommer, J. *Angew. Chem., Int. Ed. Engl.* **1992**, *31*, 1298. Tsukruk, V. V.; Reneker, D. H. *Polymer*, submitted.
(16) Overney, R. M.; Meyer, E.; Frommer, J.; Güntherot, H. J.; Decher, G.; Reibel, J.; Sohling, U. *Langmuir* **1993**, *9*, 341.
(17) Duda, G.; Schouten, A. J.; Arndt, T. J.; Lieser, G.; Schmidt, G. F.; Bubeck, C.; Wegner, G. *Thin Solid Films* **1988**, *159*, 221.
(18) Vierheller, T. R.; Foster, M. D.; Schmidt, A.; Mathauer, K.; Knoll, W.; Wegner, G.; Satija, S.; Majkrzak, C., in preparation.
(19) Leung, O. M.; Goh, M. G. *Science* **1992**, *255*, 64. Meyers, G. F.; DeKoven, B. M.; Seitz, J. T. *Langmuir* **1992**, *8*, 2330.
(20) Yoshizawa, H.; McGuiggan, P.; Israelachvili, J. *Science* **1993**, *259*, 1305. Yoshizawa, H.; Chen, Y.-L.; Israelachvili, J. *J. Phys. Chem.* **1993**, *97*, 4128. Yoshizawa, H.; Israelachvili, J. *J. Phys. Chem.*, to be submitted.
(21) Robbins, M. O.; Thompson, P. A. *Science* **1991**, *253*, 916.
(22) Schmidt, A. Thesis, University of Mainz, 1993.
(23) Harrison, J. A.; White, C. T.; Colton, R. J.; Brenner, D. W. *Phys. Rev.* **1992**, *B46*, 9700.
(24) Tsukruk, V. V.; Shilov, V. V. *Structure of Polymer Liquid Crystals*; Naukova Dumka: Kiev, 1990.
(25) Vierheller, T. R.; Wu, H.; Foster, M. D.; Schmidt, A., in preparation.
(26) Hiemenz, P. C. *Principles of Colloid and Surface Chemistry*; Marcel Dekker: New York, 1986.